



## Adsorption and removal of bisphenol A from aqueous solution by *p*-phenylenediamine-modified magnetic graphene oxide

XIAOSHENG TANG<sup>1</sup>, PING TANG<sup>2,3</sup>, SHIHUI SI<sup>4</sup> and LIANGLIANG LIU<sup>2\*</sup>

<sup>1</sup>Hubei Key Laboratory of Edible Wild Plants Conservation and Utilization & College of Life Sciences, Hubei Normal University, Huangshi, Hubei 435002, China, <sup>2</sup>Institute of Bast Fiber Crops, Chinese Academy of Agricultural Sciences, Changsha 410205, China, <sup>3</sup>School of Environmental Science and Engineering, Hubei Polytechnic University, Hubei Key Laboratory of Mine Environmental Pollution Control and Remediation, Huangshi, Hubei 435003, China and <sup>4</sup>College of Chemistry and Chemical Engineering, Central South University, Changsha, Hunan 410083, China

(Received 30 April, revised 17 September, accepted 10 October 2016)

**Abstract:** *p*-Phenylenediamine-functionalized magnetic graphene oxide nanocomposites (PPD–MGO) were prepared and utilized in the adsorption and removal of bisphenol A from aqueous solution. The novel nanomaterials were characterized by transmission electron microscopy (TEM), Fourier transform infrared spectroscopy (FT-IR) and a vibrating sample magnetometer (VSM). The factors affecting the adsorption of bisphenol A, including adsorption time, temperature and pH of solution, adsorption kinetics and isotherms were all investigated. The results showed that the PPD–MGO nanomaterial exhibited good adsorption ability for bisphenol A and good re-usability. The maximum adsorption capacity reached 155.0 mg g<sup>-1</sup> at 45 °C and pH 7. The removal rate was 99.2 % after three times adsorption with the new nanomaterials. After five adsorption cycles, the adsorption capacity of the PPD–MGO remained at 94.0 %. The adsorption of bisphenol A was found to fit pseudo second order kinetics equations and the Freundlich adsorption model. The experimental results showed the PPD–MGO nanomaterial had a good adsorption ability to remove organic compounds from aqueous solution.

**Keywords:** adsorption; bisphenol A; graphene oxide; magnetic nanoparticles.

### INTRODUCTION

With the development of modern industry in these years, water pollution has become a universal crisis.<sup>1</sup> Continuous concern for public and environmental health has led to increasing interest in treating toxic organic and inorganic pollutants in water.<sup>2</sup> Moreover, many new chemical compounds have been iden-

\*Corresponding author. E-mail: liuliangliang@caas.cn  
doi: 10.2298/JSC160430095T

tified as harmful to the environment. Endocrine disrupting compounds (EDCs) are derived from various kinds of chemicals, including drugs, pesticides, consumer products, and pollutants.<sup>3</sup> EDCs are harmful to human health and the ecological environment, and could result in bio-accumulation and reproductive toxicity. It was reported that EDCs disturb the human endocrine system by mimicking, blocking or disrupting the functions of hormones.<sup>4</sup>

Bisphenol A (BPA), classified as a type of EDC, is widely used in the production of polycarbonates, epoxy resins, plasticizers, flame retardants and other chemical products.<sup>5</sup> Since BPA at low concentrations could cause infertility and breast cancer, wastewater containing BPA has to be treated adequately before being discharged into environment.<sup>6</sup> The development of a rapid and efficient method for removal of BPA is therefore of considerable importance.

Nowadays, many techniques have been applied in water treatment. Among these techniques, adsorption seems to be the most extensively utilized and economically feasible method, possessing a relatively high capacity and low cost.<sup>7</sup> Various nanomaterials have been used as adsorbents for the removal of toxic pollutant from water in recent years.<sup>8–11</sup> Graphene oxide (GO) is a novel two-dimensional nanomaterial prepared from graphite. It has attracted significant attention in wastewater treatment due to its high mechanical strength and ease of functionalization.<sup>12</sup> GO contains abundant hydrophilic oxygen-containing functional groups on its basal planes and edges, which provide GO with a highly efficient adsorption ability.<sup>13</sup> Therefore, GO could serve as an ideal adsorption material because of its large specific surface area, abundant groups and high water solubility.<sup>14,15</sup> Magnetic nanomaterials have drawn much attention in adsorption and separation because they are easily separated from the solution and recycled. The magnetic properties of magnetic nanomaterials enable separation using a magnet instead of filtration, centrifugation or decantation.<sup>16,17</sup> Magnetic nanomaterials have been used as adsorbents for the adsorption and removal of toxic compounds in aqueous solution, especially after modification.<sup>18</sup> GO-based magnetic nanomaterials were also widely used in pollution control.<sup>19–22</sup> The combination of magnetic materials and GO could significantly simplify the separation process and increase the adsorption capacity.

In this study, *p*-phenylenediamine (PPD)-functionalized magnetic nanoparticles (PPD–MN) were successfully synthesized and bound onto GO, and the PPD-functionalized magnetic GO (PPD–MGO) was applied in the adsorption and removal of BPA. The existence of PPD could increase the interaction between adsorbent and target compounds because of the introduction of phenyl groups and amino groups. The effects of pH, temperature and adsorption time on the adsorption of BPA, the re-usability of PPD–MGO and removal of BPA were investigated. The kinetics and isotherm parameters of the adsorption were

determined and calculated. The experimental results showed PPD–MGO had a high adsorption capacity and could be easily re-used.

## EXPERIMENTAL

### Chemicals and materials

Bisphenol A (BPA), *p*-phenylenediamine (PPD), glutaraldehyde, *N*-hydroxyl succinimide (NHS), 1-ethyl-3-(3-dimethylaminopropyl) carbodiimide hydrochloride (EDC), and 3-amino-propyltriethoxysilane were purchased from Sigma–Aldrich. Ferric chloride hexahydrate ( $\text{FeCl}_3 \cdot 6\text{H}_2\text{O}$ ) and poly(ethylene glycol) (PEG 6000) were purchased from Sinopharm Chemical Reagents. Ultrapure water (18.2 M $\Omega$  cm resistivity) was obtained from a Milli-Q water purification system. All other reagents used in this study were of analytical grade.

### Preparation of PPD–MGO

*Preparation of PPD functionalized  $\text{Fe}_3\text{O}_4$  nanoparticles (PPD–MN).*  $\text{FeCl}_3 \cdot 6\text{H}_2\text{O}$  (1.350 g), PEG 6000 (1.000 g) and anhydrous sodium acetate (3.600 g) were mixed in ethylene glycol (40 mL) under stirring for 30 min. The mixture was transferred to a stainless steel autoclave and maintained at 180 °C for 8 h. Finally, the black  $\text{Fe}_3\text{O}_4$  nanoparticles were obtained by magnetic separation, washed with ethanol three times and dried under vacuum at 40 °C for 2 h. The  $\text{Fe}_3\text{O}_4$  nanoparticles (0.100 g) were then added into an ethanol solution (200 mL, 99.5 %) with mechanical agitation. After 30 min reaction, 3-aminopropyltriethoxysilane (2.0 mL) was slowly added and the solution was stirred at room temperature for 6 h. The obtained amino  $\text{Fe}_3\text{O}_4$  nanoparticles were washed with ethanol three times and dried under vacuum at 40 °C for 2 h. The amino  $\text{Fe}_3\text{O}_4$  nanoparticles (0.100 g) were added into a glutaraldehyde solution (20 mL, 5 vol. %) and stirred for 30 min. Then PPD solution (5 mL, 20 mg mL $^{-1}$ ) was added to the mixture and stirred. After further 30 min reaction, the excess PPD was removed by magnetic separation and the PPD–MN was washed three times with ethanol. The PPD–MN was dried under vacuum at 40 °C for 2 h.

*Preparation of GO.* GO was prepared according to the improved synthetic method reported by Marcano.<sup>23</sup> Concentrated  $\text{H}_2\text{SO}_4$  (120 mL),  $\text{H}_3\text{PO}_4$  (13 mL), graphite flakes (1.000 g) and  $\text{KMnO}_4$  (6.000 g) were mixed and heated at 50 °C for 12 h with magnetic stirring. Then the mixture was poured into ice (130 mL) containing 3 mL of 30 %  $\text{H}_2\text{O}_2$  and centrifuged (8000 rpm) for 1 h. The supernatant was decanted and the solid material was washed with 30 % HCl and water five times respectively under the same centrifugation conditions. Finally, the obtained solid material was dried under vacuum at 40 °C for 6 h.

*Preparation of PPD–MGO.* EDC (5 mL, 5 mg mL $^{-1}$ ) and NHS (5 mL, 5 mg mL $^{-1}$ ) were added to a solution of GO (50 mL, 2 mg mL $^{-1}$ ) under continuous stirring to activate the carboxyl groups of GO.<sup>24</sup> PPD–MN (0.200 g) was then added and dispersed ultrasonically for 30 min. The obtained product was collected by magnetic separation and dried in vacuum at 40 °C for 4 h.

### Characterizations of PPD–MGO

PPD–MGO and GO were characterized using a JEOL200CX electron microscope (Jeol, Tokyo, Japan) at 160 kV for TEM images. FT-IR spectra were obtained using a Nicolet avatar 360 FT-IR spectrophotometer (Thermo Fisher Nicolet, Orlando, USA). The magnetic property was investigated at room temperature using a Lakeshore 7407 vibrating sample magnetometer (VSM, Westerville, Ohio, USA).

### *Adsorption of BPA*

PPD–MGO (5 mg) was added to solutions (20 mL) containing different concentrations of BPA and the mixtures were shaken for 120 min at 25, 35 and 45 °C. The mixtures were separated with a magnet and the concentration of BPA was monitored by UV–Vis spectrophotometer (UV-2600, Shimadzu, Kyoto, Japan) at 276 nm. For comparison, the same amount of Fe<sub>3</sub>O<sub>4</sub> nanoparticles, GO, PPD–MN and PPD–MGO (5 mg) were added to BPA solution (20 mL, 250 mg L<sup>-1</sup>) and the mixtures were shaken for 120 min at 25 °C. The mixture was separated with a magnet or centrifugation and the concentration of BPA was monitored by UV–Vis spectrophotometry at 276 nm. To study the effects of the initial pH on the adsorption of BPA, the initial pH value of the solution was adjusted to 5.0–9.0 by addition of hydrochloric acid or sodium hydroxide. All experiments were performed in triplicate.

### *Adsorption kinetics*

PPD–MGO (5 mg) and BPA solution (20 mL, 100 mg L<sup>-1</sup>) were mixed and shaken at 25 °C. The concentration of BPA was monitored by UV–Vis spectrophotometry at certain intervals. In order to study the mechanism of the adsorption kinetics, the pseudo-first-order kinetic model and the pseudo-second-order kinetic models were used.

The pseudo-first-order kinetic model could be expressed by the following equation:

$$\ln(q_e - q_t) = \ln q_e - k_1 t \quad (1)$$

where  $q_e$  (mg g<sup>-1</sup>) is the equilibrium adsorption capacity,  $q_t$  (mg g<sup>-1</sup>) is the amount of adsorbed at time  $t$ ,  $k_1$  (g mg<sup>-1</sup> min<sup>-1</sup>) is the rate constant of adsorption.

The pseudo-second-order kinetic model could be expressed by the following equation:

$$\frac{t}{q_t} = \frac{1}{k_{ad} q_e^2} + \frac{1}{q_e} t \quad (2)$$

where  $k_{ad}$  (g mg<sup>-1</sup> min<sup>-1</sup>) is the rate constant of adsorption,  $q_e$  (mg g<sup>-1</sup>) is the equilibrium adsorption capacity,  $q_t$  (mg g<sup>-1</sup>) is the amount adsorbed at time  $t$ .<sup>25</sup>

### *Adsorption isotherm*

PPD–MGO (5 mg) was added to BPA solution (20 mL) at a concentration in the range of 75–250 mg L<sup>-1</sup>. The mixtures were shaken at 25, 35 and 45 °C for 120 min and the concentration of BPA was determined. The Langmuir and Freundlich isotherm<sup>26</sup> models were used to evaluate the adsorption isotherm.

### *Reusability of PPD–MGO*

To study the reusability, PPD–MGO (5 mg) was added to a BPA solution (20 mL, 100 mg L<sup>-1</sup>) and shaken for 120 min at 45 °C. The mixture was then separated with a magnet and the concentration of BPA was determined. The recycle of PPD–MGO was obtained by washing with ethanol and water three times. Then the recycled PPD–MGO was added into another BPA solution to start a new adsorption. All the experiments were performed in triplicate.

## RESULTS AND DISCUSSION

### *Characterization of PPD–MGO*

The TEM images of GO and PPD–MGO are presented in Fig. 1. The sheet structure with smooth surface and wrinkled edges of GO could be found in Fig. 1a. It also could be seen that PPD–MN was bound with GO and the shape of GO

changed in Fig. 1b. The mean diameter of the  $\text{Fe}_3\text{O}_4$  nanoparticles was about 200 nm. These characteristics of GO and the shape of  $\text{Fe}_3\text{O}_4$  nanoparticles could also be found in reported related research.<sup>27,28</sup> It could be considered that PPD–MGO was successfully fabricated.

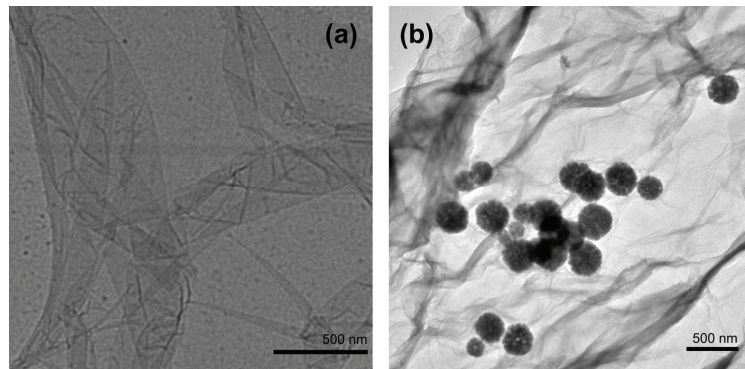


Fig. 1. TEM images of (a) GO and (b) PPD–MGO.

The FT-IR spectra of  $\text{Fe}_3\text{O}_4$  nanoparticles, PPD–MN, GO and PPD–MGO are presented in Fig. 2. The FT-IR spectrum of the  $\text{Fe}_3\text{O}_4$  nanoparticles showed the major characteristic peak at  $572 \text{ cm}^{-1}$ . The FT-IR spectrum of PPD–MN showed featured absorptions due to the presence of PPD. The absorptions at  $3423, 1510, 1083$  and  $821 \text{ cm}^{-1}$  could be identified as N–H stretching vibrations, the skeleton vibration of the benzenoid ring, and the in-plane and out-of-plane bending vibrations of C–H, respectively.<sup>29,30</sup> Additionally, the weak band at  $2921 \text{ cm}^{-1}$  was associated with C–H stretching vibrations. The bands at  $1627$

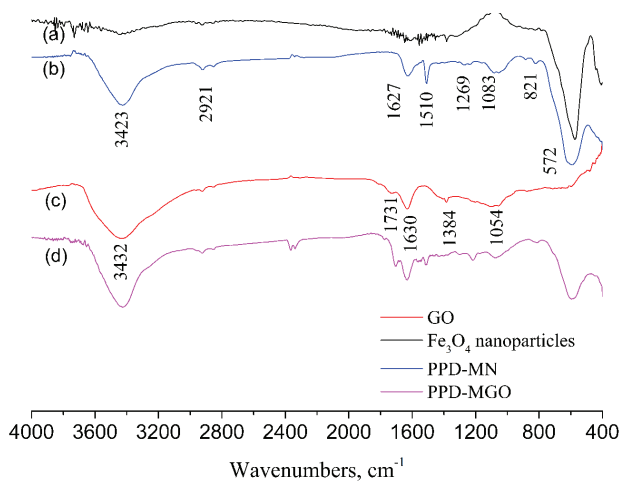


Fig. 2. FT-IR spectra of: a)  $\text{Fe}_3\text{O}_4$  nanoparticles, b) PPD–MN, c) GO and d) PPD–MGO.

$\text{cm}^{-1}$  and  $1296 \text{ cm}^{-1}$  were assigned to C–N stretching vibrations.<sup>31</sup> The spectrum of PPD–MN also showed the characteristic peak at around  $580 \text{ cm}^{-1}$ , assigned to Fe–O vibrations. The FT-IR spectrum of GO showed absorptions at 3432, 1731 and  $1630 \text{ cm}^{-1}$ , assigned to hydroxyl, carbonyl and  $\text{sp}^2$ -bonded carbon groups on the GO, respectively.<sup>32,33</sup> The absorptions at  $1054 \text{ cm}^{-1}$  and  $1384 \text{ cm}^{-1}$  were considered as the C–O stretching peak and O–H deformation peak.<sup>32</sup> All the feature peaks of the spectra of GO and PPD–MN could be observed in the spectrum of PPD–MGO. It could be assumed that PPD–MGO was successfully synthesized.

The VSM characterization of the  $\text{Fe}_3\text{O}_4$  nanoparticles and PPD–MGO were conducted at room temperature to confirm the magnetic properties. As shown in Fig. 3, the saturation magnetization values of the  $\text{Fe}_3\text{O}_4$  nanoparticles and PPD–MGO were 71.7 and  $33.6 \text{ emu g}^{-1}$ , respectively. Compared to  $\text{Fe}_3\text{O}_4$  nanoparticles, the decrease in the saturation magnetization value of PPD–MGO could be attributed to the existence of non-magnetic materials.<sup>34,35</sup> The sufficient magnetic response and almost zero remanence of PPD–MGO guaranteed the materials for magnetic separation with an ordinary magnet.

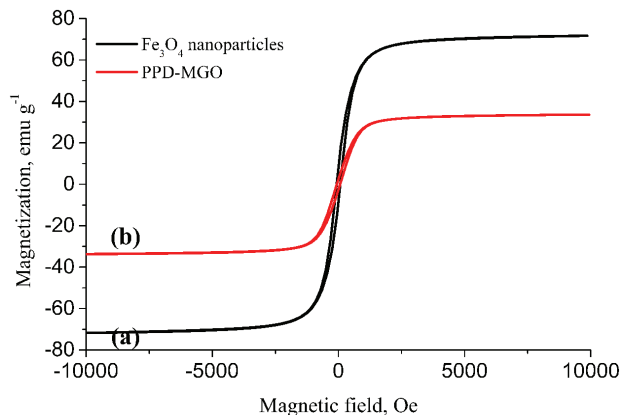


Fig. 3. Magnetization curve of: a)  $\text{Fe}_3\text{O}_4$  nanoparticles and b) PPD–MGO.

In order to confirm the adsorption capacity of PPD–MGO, the adsorption of BPA with  $\text{Fe}_3\text{O}_4$  nanoparticles, GO, PPD–MN and PPD–MGO were conducted and compared under the same condition. The adsorption capacities of  $\text{Fe}_3\text{O}_4$  nanoparticles, GO, PPD–MN and PPD–MGO at  $25^\circ\text{C}$  were 40.4, 108.3, 62.8 and  $151.6 \text{ mg g}^{-1}$ , respectively. It was found that the adsorption capacity was increased after the modification of PPD and the combination between GO and PPD–MN. As adsorption is a surface phenomenon, the adsorbent with a higher surface area leads to a higher adsorption capacity. The excellent adsorption ability of PPD–MGO is the result of its large surface area (theoretical surface

area up to  $2675\text{ m}^2\text{ g}^{-1}$ ) and its abundance of carboxyl, hydroxyl and epoxy groups.<sup>36–38</sup>

#### *Effect of pH*

The pH of a solution plays an important role in adsorption processes. It affects the adsorption capacity of an adsorbent and electrostatic interaction between compounds and the adsorbent surface. The effect of pH on the adsorption of BPA was investigated at different pH values, ranging from 5.0 to 9.0. As shown in Fig. 4, the adsorption capacity reached a maximum when the pH was 7.0 and then decreased with increasing pH.<sup>39</sup> The decrease in the adsorption capacity for BPA might be due to deprotonation of the hydroxy of phenol when the pH was above 7.<sup>40</sup> The adsorptive effect might be mediated by hydrogen bonding between BPA and PPD–MGO and by hydrophobic adsorption.<sup>41,42</sup> Therefore, the optimum pH for adsorption of BPA was set at 7.0.

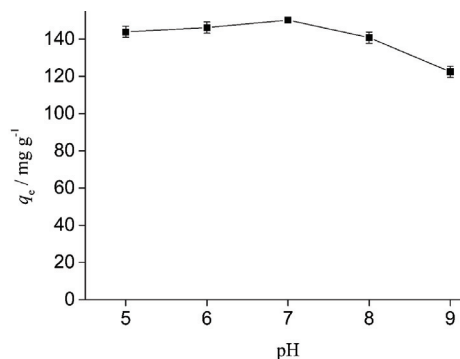


Fig. 4. The influence of the initial pH value on the adsorption of BPA.

#### *Adsorption kinetics*

The data related to kinetics of BPA adsorption on PPD–MGO are shown in Fig. 5a. The concentration of BPA decreased significantly in the first 30 min, and then the decrease trended to slow down until the adsorption equilibrium was achieved. When the incubation time exceeded 120 min, no increase in the adsorbed amount was apparent. Considering the efficiency of the experiments, an adsorption time for the experiments was selected to be 120 min.

The adsorption of BPA was fitted with the pseudo-first-order and pseudo-second-order kinetic equations. The corresponding results are shown in Fig. 5b and c, respectively. For the pseudo-first-order equation, the constant  $k_1$  was calculated as  $0.0343\text{ g mg}^{-1}\text{ min}^{-1}$  and the correlation coefficient of fitting the model was 0.996, while the constant  $k_{ad}$  in the pseudo-second-order kinetic equation was calculated as  $0.0055\text{ g mg}^{-1}\text{ min}^{-1}$  and the correlation coefficient of fitting the model reached 0.999. The results indicated that the adsorption of BPA on PPD–MGO fitted better with the pseudo-second-order kinetic equation. It

could be suggested that the adsorption behavior of BPA onto PPD–MGO was promoted by a chemical process involving valence forces through sharing or exchange of electrons between sorbent and sorbate as covalent forces.<sup>43</sup> This means that the sorption of BPA on PPD–MGO might be due to chemical reaction between the negative charge on PPD–MGO and the positive charge on the BPA molecules.<sup>44</sup>

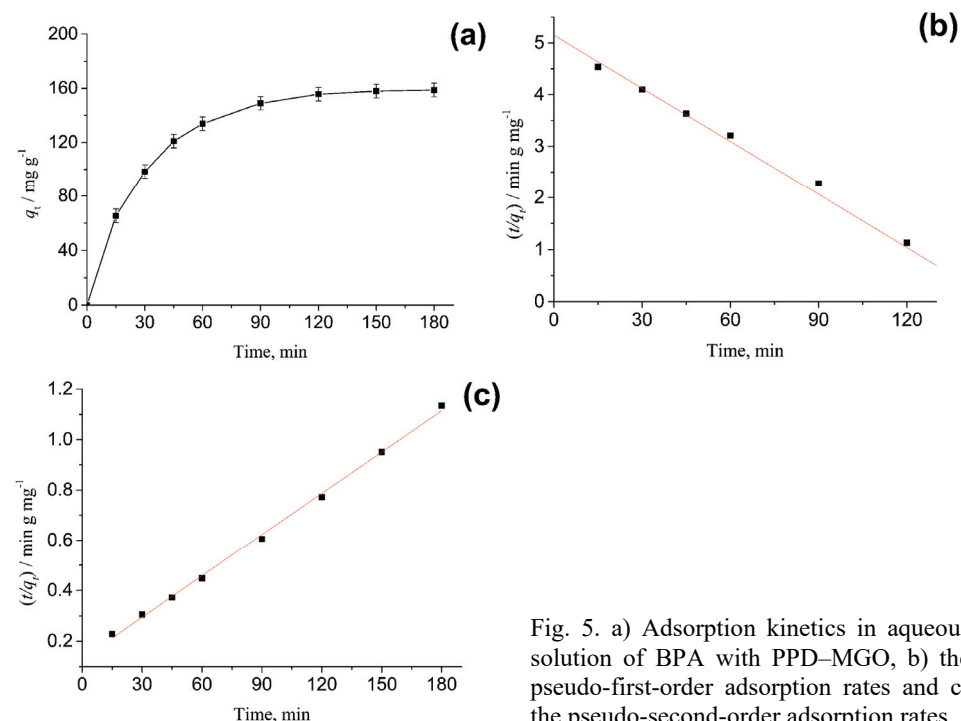


Fig. 5. a) Adsorption kinetics in aqueous solution of BPA with PPD–MGO, b) the pseudo-first-order adsorption rates and c) the pseudo-second-order adsorption rates.

#### *Adsorption isotherm*

Adsorption isotherm is important for investigating the adsorption behavior of an adsorbent. The correlation between the experimental equilibrium data and theoretical model is also essential for the interpretation of the adsorption. In this study, the isotherm data for the adsorption of BPA on PPD–MGO were fitted with the Langmuir and Freundlich models. The adsorption isotherms are shown in Fig. 6 and the parameters of the Langmuir and Freundlich models were listed in Table I. Apparently, the coefficient of correlation of Freundlich model was higher than that of Langmuir model. The Freundlich isotherm model can be used to describe sorption on heterogeneous surfaces and multilayer sorption formation.<sup>45</sup> Therefore, compared to the Langmuir model, the adsorption of BPA on PPD–MGO was more coincident with the Freundlich model.

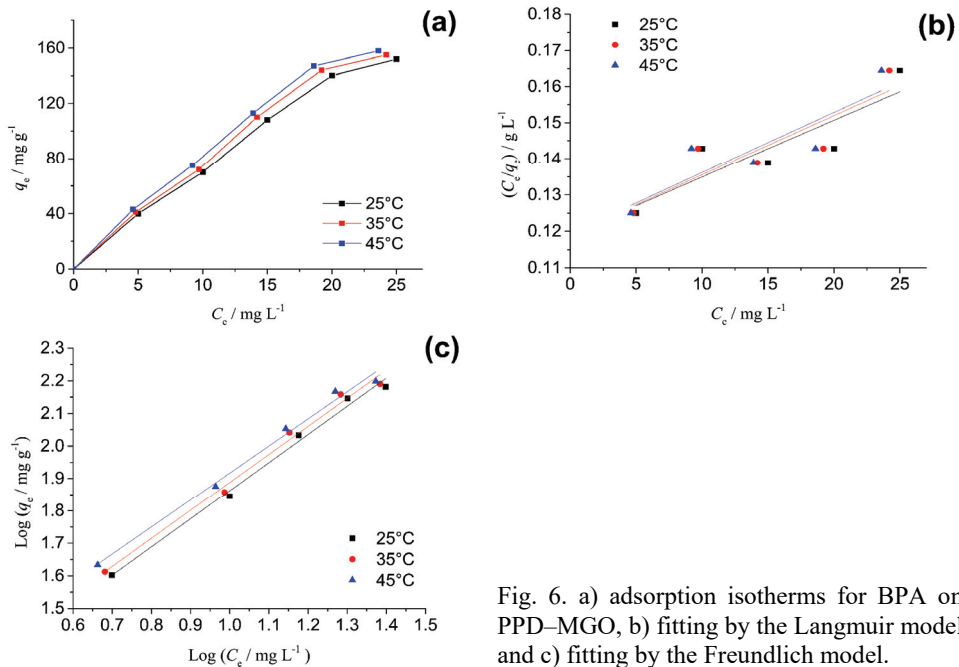


Fig. 6. a) adsorption isotherms for BPA on PPD–MGO, b) fitting by the Langmuir model and c) fitting by the Freundlich model.

TABLE I. Isotherm parameters for the adsorption of BPA on PPD–MGO

Model	Parameter	$t / ^\circ C$		
		25	35	45
Langmuir	$q_m / mg g^{-1}$	152.0	155.0	158.0
	$b$	0.0552	0.0542	0.0551
	$R^2$	0.703	0.7177	0.7114
Freundlich	$1/n$	0.8328	0.8627	0.8665
	$K / mg g^{-1}$	12.1367	10.5974	9.9038
	$R^2$	0.9882	0.9863	0.9896

#### Reusability of PPD–MGO and removal of BPA

The reusability of an adsorbent is important in practical applications. The recycling of an adsorbent would reduce the cost of the adsorbent and the impact of the adsorbent on the environment.<sup>46</sup> The results of the reusability test of PPD–MGO are shown in Fig. 7. During five cycles of use, a small drop in the adsorption capacity of PPD–MGO could be observed. However, the adsorption capacity of PPD–MGO remained at 141.0 mg g<sup>-1</sup> (94 % of the initial adsorption capacity) after five cycles. These results showed that PPD–MGO exhibited satisfactory reusability in adsorption.

The removal of BPA with successive cycles of PPD–MGO was conducted. After one cycle adsorption, the adsorbent was separated with a magnet and new

PPD–MGO was added to start the next cycle of adsorption. The removal efficiency was calculated using the following equation:

$$\text{Removal efficiency, \%} = 100 \left( 1 - \frac{c_e}{c_0} \right) \quad (5)$$

where  $c_e$  ( $\text{mg L}^{-1}$ ) is the equilibrium concentration of BPA and  $c_0$  ( $\text{mg L}^{-1}$ ) is the initial concentration of BPA. The removal efficiency of BPA with successive new PPD–MGO could reach 99.2 % after three cycles (Fig. 8). These results showed that the prepared adsorbents could effectively remove BPA from the environment.

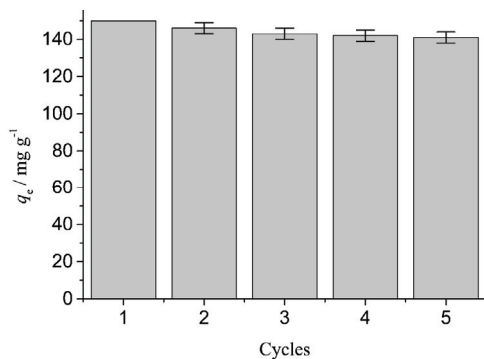


Fig. 7. Reusability of PPD–MGO.

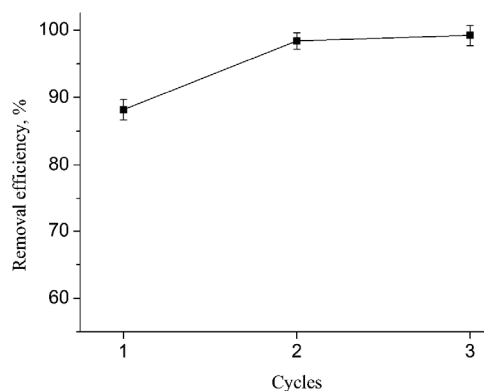


Fig. 8. Removal of BPA using PPD–MGO.

## CONCLUSIONS

In summary, PPD–MGO was successfully prepared and characterized. The adsorption kinetics and isotherms were investigated in detail. The adsorption of BPA followed pseudo-second-order kinetics and the equilibrium data were fitted well with the Freundlich isotherm model. PPD–MGO also showed good reusability in the adsorption and BPA could be effectively removed by three times

successive adsorptions. In conclusion, PPD–MGO could be a competitive candidate with great potential applications for the removal of BPA from water.

*Acknowledgements.* This work was supported by Science and Technology Research Project of Hubei Province Education Department (B2016164).

#### ИЗВОД

#### АДСОРПЦИЈА И УКЛАЊАЊЕ БИСФЕНОЛА А ИЗ ВОДЕНИХ РАСТВОРА ПРИМЕНОМ МАГНЕТНОГ ГРАФЕН-ОКСИДА МОДИФИКОВАНОГ *p*-ФЕНИЛЕНДИАМИНОМ

XIAOSHENG TANG<sup>1</sup>, PING TANG<sup>2,3</sup>, SHIHUI SI<sup>4</sup> и LIANGLIANG LIU<sup>2</sup>

<sup>1</sup>Hubei Key Laboratory of Edible Wild Plants Conservation and Utilization & College of Life Sciences, Hubei Normal University, Huangshi, Hubei 435002, China, <sup>2</sup>Institute of Bast Fiber Crops, Chinese Academy of Agricultural Sciences, Changsha 410205, China, <sup>3</sup>School Of Environmental Science and Engineering, Hubei Polytechnic University, Hubei Key Laboratory of Mine Environmental Pollution Control and Remediation, Huangshi, Hubei 435003, China и <sup>4</sup>College of Chemistry and Chemical Engineering, Central South University, Changsha, Hunan 410083, China

Нанокомпозити магнетног графен-оксида функционализованог *p*-фенилендиамином (PPD–MGO) су припремљени и коришћени за адсорпцију и уклањање бисфенола А из водених растворова. Нови наноматеријали су охарактерисани трансмисионом електронском микроскопијом (TEM), инфрацрвеном спектроскопијом са Фуријевом трансформацијом (FT-IR) и магнетометром са вибраирајућим узорком (VSM). Адсорпција бисфенола А је испитивана праћењем времена адсорпције, температуре, pH раствора, адсорpcione кинетике и изотерми. Резултати су показали да је PPD–MGO наноматеријал добар адсорбент бисфенола А и да је могућа његова вишеструка примена као адсорбента. Максимални адсорpcionи капацитет био је 155,0 mg g<sup>-1</sup> на 45 °C и pH 7. Степен уклањања је био 99,2 % након три пута поновљене адсорпције са новим наноматеријалима. После пет циклуса адсорпције, адсорpcionи капацитет PPD–MGO је остао 94,0 %. Адсорпција бисфенола А пратила је кинетику псевдо другог реда и Фројндлихову адсорpcionу изотерму. Експериментали резултати су показали да PPD–MGO наноматеријал има добре адсорpcione карактеристике за уклањање органских једињења из водених растворова.

(Примљено 30. априла, ревидирано 17. септембра, прихваћено 10. октобра 2016)

#### REFERENCES

1. O. N. Kononova, N. S. Karpelyakova, E. V. Duba, *J. Serb. Chem. Soc.* **80** (2015) 1149
2. Ö. Demirbaş, Y. Turhan, M. Alkan, *Desalin. Water Treat.* **54** (2015) 707
3. P. Westerhoff, Y. Yoon, S. Snyder, E. Wert, *Environ. Sci. Technol.* **39** (2005) 6649
4. M. J. Benotti, R. A. Trenholm, B. J. Vanderford, J. C. Holady, B. D. Stanford, S. A. Snyder, *Environ. Sci. Technol.* **43** (2009) 597
5. J. Xu, L. Wang, Y. F. Zhu, *Langmuir* **28** (2012) 8418
6. C. S. Guo, M. Ge, L. Liu, G. D. Gao, Y. C. Feng, Y. Q. Wang, *Environ. Sci. Technol.* **44** (2010) 419
7. G. Bayramoglu, M. Y. Arica, G. Liman, O. Celikbicak, B. Salih, *Chemosphere* **150** (2016) 275
8. J. Wang, Q. Zhou, D. Song, B. Qi, Y. Zhang, Y. Shao, Z. Shao, *J. Sol-Gel Sci. Technol.* **76** (2015) 1
9. J. Shen, Z. Li, Y. N. Wu, B. Zhang, F. Li, *Chem. Eng. J.* **264** (2015) 48
10. H. Hosseinzadeh, S. Zoroufi, G. R. Mahdavinia, *Polym. Bull.* **72** (2015) 1339

11. Y. Wang, M. Yao, Y. Chen, Y. Zuo, X. Zhang, L. Cui, *J. Alloys Compd.* **627** (2015) 7
12. Y. Wang, Z. Li, J. Wang, J. Li, Y. Lin, *Trends Biotechnol.* **5** (2011) 205
13. M. Q. Yang, J. H. He, *Sensors Actuators, B* **228** (2016) 486
14. D. A. Dikin, S. Sasha, E. J. Zimney, R. D. Piner, G. H. B. Dommett, E. Guennadi, S. B. T. Nguyen, R.S. Ruoff, *Nature* **448** (2007) 457
15. D. R. Dreyer, S. J. Park, C. W. Bielawski, R. S. Ruoff, *Chem. Soc. Rev.* **39** (2010) 228
16. J. Wang, Z. Y. Chen, Z. M. Li, Y. L. Yang, *Food Chem.* **204** (2016) 135
17. M. L. Wang, G. D. Fang, P. Liu, D. M. Zhou, C. Ma, D. J. Zhang, J. H. Zhan, *Appl. Catal., B* **188** (2016) 113
18. A. H. Lu, E. L. Salabas, S. Ferdi, *Angew. Chem. Int. Ed.* **46** (2007) 1222
19. Z. Ruizhe, S. Ping, Y. Yi, *J. Sep. Sci.* **37** (2014) 3339
20. H. Teymourian, A. Salimi, S. Khezrian, *Biosens. Bioelectron.* **49c** (2013) 1
21. K. C. Zhang, Y. F. Li, Y. Liu, Y. Zhu, *Carbon* **102** (2016) 39
22. M. Fu, J. Li, *Nanosci. Nanotechnol. Lett.* **6** (2014) 1116
23. D. C. Marcano, D. V. Kosynkin, J. M. Berlin, A. Sinitskii, Z. Sun, A. Slesarev, L. B. Alemany, W. Lu, J. M. Tour, *ACS Nano* **4** (2010) 4806
24. S. Roy, N. Soin, R. Bajpai, D. S. Misra, J. A. McLaughlin, S. S. Roy, *J. Mater. Chem.* **21** (2011) 14725
25. R. Sivashankar, A. B. Sathya, U. Krishnakumar, V. Sivasubramanian, *Ecotoxicol. Environ. Saf.* **121** (2015) 149
26. P. Chakraborty, R. Nagarajan, *Appl. Clay Sci.* **118** (2015) 308
27. M. Bhadra, S. Roy, S. Mitra, *Desalination* **378** (2016) 37
28. H. Deng, X. Li, Q. Peng, X. Wang, J. Chen, Y. Li, *Angew. Chem. Int. Ed.* **117** (2005) 2842
29. S. Liu, B. Yu, T. Zhang, *J. Mater. Chem., A* **1** (2013) 13314
30. Y. Zheng, Y. Liu, A. Wang, *Ind. Eng. Chem. Res.* **51** (2012) 10079
31. X. Tian, W. Wang, N. Tian, C. Zhou, C. Yang, S. Komarneni, *J. Hazard. Mater.* **309** (2016) 151
32. Y. Xu, H. Bai, G. Lu, C. Li, G. Shi, *J. Am. Chem. Soc.* **130** (2008) 5856
33. Y. Jin, S. Huang, M. Zhang, M. Jia, *Synth. Met.* **168** (2013) 58
34. T. Eslaminejad, S. N. Nematollahi-Mahani, M. Ansari, *J. Magn. Magn. Mater.* **402** (2016) 34
35. P. P. Waifalkar, S. B. Parit, A. D. Chougale, S. C. Sahoo, P. S. Patil, P. B. Patil, *J. Colloid Interface Sci.* **482** (2016) 159
36. D. Wang, L. Liu, X. Jiang, J. Yu, X. Chen, *Colloids Surfaces, A* **466** (2015) 166
37. Z. Yuan, H. Tai, Z. Ye, C. Liu, G. Xie, X. Du, Y. Jiang, *Sensors Actuators, B-Chem.* **234** (2016) 145
38. C. Bussy, H. Ali-Boucetta, K. Kostarelos, *Acc. Chem. Res.* **46** (2013) 692
39. G. Xiao, L. Fu, A. Li, *Chem. Eng. J.* **191** (2012) 171
40. R. Sohrabi, N. Bahramifar, H. Javadian, S. Agarwal, V. K. Gupta, *Biomed. Chromatogr.* **30** (2016) 1256
41. W. Su-Hua, D. Bing-Zhi, H. Yu, *Desalination* **253** (2010) 22
42. S. Li, Y. Gong, Y. Yang, C. He, L. Hu, L. Zhu, L. Sun, D. Shu, *Chem. Eng. J.* **260** (2015) 231
43. A. C. Arampatzidou, E. A. Deliyanni, *J. Colloid Interface Sci.* **466** (2016) 101
44. A. E. Ofomaja, *Biochem. Eng. J.* **40** (2008) 8
45. F. Qiu, M. Peng, Z. Wei, X. Wang, J. Yang, *J. Appl. Polym. Sci.* **133** (2016) 43066
46. F. Duan, C. Chen, X. Zhao, Y. Yang, X. Liu, Y. Qin, *Environ. Sci. Nano* **3** (2016) 213.